

Indirect and direct signatures of Higgs portal decaying vector dark matter for positron excess in cosmic rays

Seungwon Baek, P. Ko, Wan-Il Park, Yong Tang

*School of Physics,
Korea Institute for Advanced Study,
Seoul 130-722, Korea*
(Dated: December 6, 2024)

Abstract

We investigate the indirect signatures of the Higgs portal $U(1)_X$ vector dark matter (VDM) X_μ from both its pair annihilation and decay. The VDM is stable at renormalizable level by Z_2 symmetry, and thermalized by Higgs-portal interactions. It can also decay by some nonrenormalizable operators with very long lifetime at cosmological time scale. If dim-6 operators for VDM decays are suppressed by 10^{16} GeV scale, the lifetime of VDM with mass ~ 2 TeV is just right for explaining the recent observed positron excess in cosmic ray using the decay of VDM into $\mu^+\mu^-$. We give one UV-complete model as an example. This scenario for Higgs portal decaying VDM with mass around ~ 2 TeV can be tested by DM direct search at XENON1T and at the future colliders by measuring the Higgs self-couplings.

Keywords:

I. INTRODUCTION

Convincing evidences of nonbaryonic dark matter (DM) exist from astrophysical scales to cosmological ones. The results from Planck [1] has already given the dark matter relic density $\Omega h^2 = 0.1199 \pm 0.0027$ with a high precision, while the standard model (SM) for particle physics has no candidate for nonbaryonic dark matter that can account for the needed relic density. We need new physics beyond SM (BSM), at least one new particle for playing the role of nonbaryonic dark matter of the universe.

Nonbaryonic dark matter must be stable on cosmological time scale and if it decays, its lifetime must be much longer than the age of the Universe. The stability of DM is usually preserved by assigning dark matter a discrete global symmetry, such as Z_2 . There are however some arguments that a global symmetry may be generically broken by quantum gravity[2, 3]. The breaking effects can lead dark matter with a global charge to decay. It can be shown that then the lifetime would be much shorter than the Universe's age based on naive dimensional analysis, if the DM mass is around electroweak scale, $\sim O(100)$ GeV – $O(1)$ TeV (see Ref. [4] for example).

A dark gauge symmetry can be used to guarantee the stability or longevity of EW scale dark matter without the above problem for global symmetry. The simplest model would be adding an extra $U(1)_X$ or some non-Abelian dark gauge symmetry to the SM gauge group G_{SM} (see Ref.s [4, 5], for example). It is also possible that hidden sector vector boson could be absolutely stable or its lifetime could be much longer than the age of the universe. Depending on the detailed model structures, the DM could be scalar, fermion or even vector particles.

One interesting scenario is the so-called Higgs portal Abelian vector dark matter (VDM) X_μ based on $U(1)_X$ Abelian dark gauge symmetry (see Ref. [6] for example), with an *ad hoc* Z_2 symmetry ($X_\mu \rightarrow -X_\mu$) that stabilizing the VDM¹. The authors of Ref. [12] emphasized that it is important to have a built-in mechanism for generating VDM mass by dark Higgs Φ . It turns out that X_μ can be the dark matter if a discrete symmetry $X_\mu \rightarrow -X_\mu$ is imposed. The new scalar Φ would interact with the SM particles due to its mixing with SM Higgs boson. There will be two neutral scalar bosons, mixtures of the SM Higgs boson and the dark Higgs boson. Due to the generic destructive interference between two scalar bosons to the amplitude for direct detection cross section, the constraint from direct detection experiments such as XENON100, CDMS and LUX are relaxed by significant amount. And the allowed model parameter space becomes larger than that in the effective model for VDM [6]. Having a dark Higgs Φ for the VDM mass, one obtains completely different results compared with the effective VDM model where the VDM mass is given by hand or by Stückelberg mechanism [6].

However, the renormalizable VDM model of Ref. [12] may not be the complete theory up to Planck scale, although the model was shown to be perturbative and the electroweak vacuum is stable up to Planck scale [12]. At some scales, $M_{GUT} \simeq 10^{16}\text{GeV}$ for instance, there could be some new physics whose symmetry breaking can induce higher dimensional operators for the low energy theory with $G_{\text{SM}} \times U(1)_X$ symmetry, which were not included in Ref. [12] (see Fig. 1). Those operators can make vector dark matter decay with a lifetime that is just at the right order in order to explain the recent observed positron excess [13–15].

In Ref. [12], most aspects of the renormalizable $U(1)_X$ VDM model have been studied in

¹ Extension with non-abelian dark gauge symmetry is also possible [7–11].

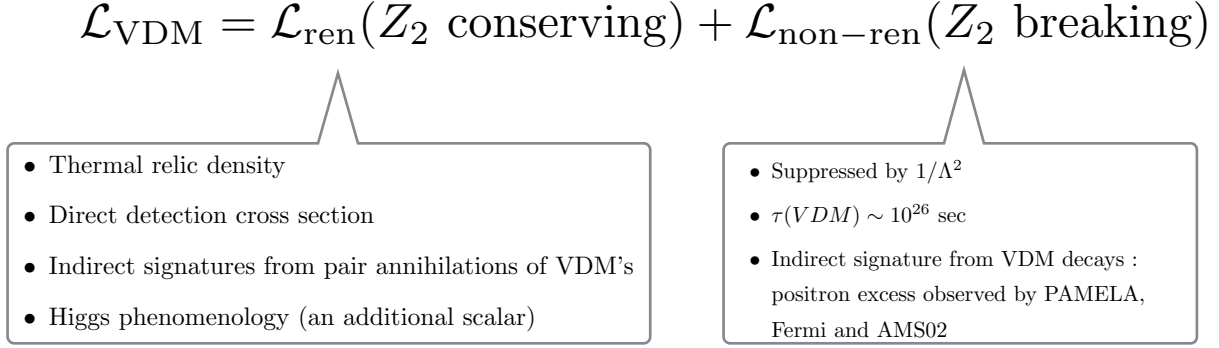


FIG. 1: Schematic view of the model Lagrangian in this work : the total Lagrangian for the VDM is a sum of the Z_2 symmetric renormalizable part and the Z_2 breaking nonrenormalizable dim-6 operators, neglecting higher dimensional operators.

detail, except for the indirect detection signals. The purpose of this work is twofold. First of all, we work out in detail various indirect signatures and compare with the cosmic ray data, such as e^+ , \bar{p} , γ or ν fluxes. There are two different sources of cosmic rays from the VDM. One is the pair annihilations of VDM's into the SM particles, which are described by Z_2 symmetric renormalizable Lagrangian of the VDM model constructed in Ref. [12]. This part will be constrained by thermal relic density, direct detection and Higgs phenomenology, as described in Ref. [12] (\mathcal{L}_{ren} in Fig. 1). The other origin is VDM decays into the SM particles², which are described by nonrenormalizable higher dimensional operators that break the ad hoc Z_2 symmetry ($\mathcal{L}_{\text{non-ren}}$ in Fig. 1). In particular we are interested in explaining the positron excess observed by PAMELA, FERMI and AMS02 [13–15]. It turns out that the pair annihilation of VDMs cannot accommodate the positron excess, because the resulting flux is too small compared with the data. Therefore we are led to consider decays of VDM by higher dimensional operators. We write down the complete list of dim-5 and dim-6 operators that cause the VDM decays into various SM particles. Among them, we select operators for VDM decays into lepton pair l^+l^- , and study the positron spectra observed by PAMELA and AMS02. We also present a simple UV completion of the nonrenormalizable operators that could account for the positron data reported by PAMELA and AMS02 Collaborations. In fact a number of works showed that PAMELA and AMS02 positron excess could be fit using $\sim 2\text{TeV}$ DM decaying into a leptons [16–36]. However their thermal relic density or direct detection cross section were (could) not studied, since these issues are independent of physics for DM decays for PAMELA and AMS02.

In this work we fill this gap by assuming that the decaying VDM for positron excess were thermalized by the Higgs portal interactions considered in Ref. [12]. If we assume that (i) these positron excess is due to the decaying VDM of mass $\sim 2\text{ TeV}$ which were thermalized by Higgs portal interactions [12], and (ii) the EW vacuum is stable up to the scale Λ where the operators for VDM decays, we find that the most parameter region could be probed by the future experiments for direct detection of WIMP's in the mass range $\sim 2\text{ TeV}$, and

² We assume that the ad hoc Z_2 symmetry of the renormalizable Lagrangian for the VDM is accidental symmetry which can be broken by higher dimensional gauge invariant operators, but not by the dim-4 kinetic mixing operators.

the Higgs self-couplings are modified. Thus we could make connection between the indirect signature for decaying VDM (with mass ~ 2 TeV) for positron excess in cosmic rays and direct detection of such heavy VDM WIMP, as well as the Higgs signal strength and the Higgs-self couplings. These predictions are newly obtained this work, compared with other works on decaying DM for positron excess reported by PAMELA, Fermi and AMS02. This accomplishes the second purpose of the present work. Although we work out in the Higgs portal VDM model in this paper, the same strategies could be applied to other types of thermal DMs.

This paper is organized as follows. In sec. II we give the detailed descriptions of the model and then give the phenomenological constraints on the parameters for a TeV X_μ in sec. III. The followed sec. IV shows some examples of the spectra for cosmic rays including gamma ray and neutrino from the pair annihilation of VDMs. In sec. V, we list the relevant higher order nonrenormalizable operators that involve both fields from the dark sector and those from the SM, and present the positron spectra from the VDM decays. We also present one UV-complete model for such a dim-6 operator, as an illustration. Then we show the positron spectra and that $X_\mu \rightarrow \mu^+ \mu^-$ could fit the positron spectra for $m_X \sim 2$ TeV, for which we identify the parameter ranges. Finally we give a summary.

II. THE MODEL

We consider a vector dark matter, X_μ , which is associated with Abelian dark gauge symmetry $U(1)_X$ implemented with discrete symmetry $X_\mu \rightarrow -X_\mu$. The simplest renormalizable and unitary model would be the one with an extra complex scalar Φ , whose vacuum expectation value (vev) is responsible for the mass of X_μ [12]:

$$\begin{aligned} \mathcal{L} = & -\frac{1}{4}X_{\mu\nu}X^{\mu\nu} + (D_\mu\Phi)^\dagger(D^\mu\Phi) - \lambda_\Phi\left(\Phi^\dagger\Phi - \frac{v_\Phi^2}{2}\right)^2 \\ & - \lambda_{H\Phi}\left(H^\dagger H - \frac{v_H^2}{2}\right)\left(\Phi^\dagger\Phi - \frac{v_\Phi^2}{2}\right) - \lambda_H\left(H^\dagger H - \frac{v_H^2}{2}\right)^2 + \mathcal{L}_{\text{SM}}. \end{aligned} \quad (2.1)$$

We here neglected the kinetic mixing term $X_{\mu\nu}B^{\mu\nu}$ which is discussed nicely in [37–40]. The above covariant derivative D_μ on Φ is defined as

$$D_\mu\Phi = (\partial_\mu + ig_X Q_\Phi X_\mu)\Phi,$$

where Q_Φ is the $U(1)_X$ charge of Φ and it can be rescaled to $|Q_\Phi| = 1$.

Assuming that the $U(1)_X$ -charged complex scalar Φ breaks $U(1)_X$ spontaneously with a nonzero vacuum expectation value (VEV) v_Φ ,

$$\Phi = \frac{1}{\sqrt{2}}(v_\Phi + \varphi),$$

the VDM X_μ gets mass equal to $M_X = g_X|Q_\Phi|v_\Phi$, and the hidden sector Higgs field (or dark Higgs field) φ will mix with the SM Higgs field $h(x)$ through Higgs portal of the $\lambda_{H\Phi}$ term. The mixing matrix O between the two scalar fields is defined as

$$\begin{pmatrix} h \\ \varphi \end{pmatrix} = \begin{pmatrix} c_\alpha & s_\alpha \\ -s_\alpha & c_\alpha \end{pmatrix} \begin{pmatrix} H_1 \\ H_2 \end{pmatrix}, \quad (2.2)$$

where $s_\alpha(c_\alpha) \equiv \sin \alpha(\cos \alpha)$, $H_i(i = 1, 2)$ are the mass eigenstates with masses M_{H_i} . H_1 will be identified as the observed 125 GeV Higgs at the LHC throughout this paper. The mass matrix in the basis (h, φ) can be written in terms of, either Lagrangian parameters or the physical parameters as follows:

$$\begin{pmatrix} 2\lambda_H v_H^2 & \lambda_{H\Phi} v_H v_\Phi \\ \lambda_{H\Phi} v_H v_\Phi & 2\lambda_\Phi v_\Phi^2 \end{pmatrix} = \begin{pmatrix} M_{H_1}^2 c_\alpha^2 + M_{H_2}^2 s_\alpha^2 & (M_{H_2}^2 - M_{H_1}^2) s_\alpha c_\alpha \\ (M_{H_2}^2 - M_{H_1}^2) s_\alpha c_\alpha & M_{H_1}^2 s_\alpha^2 + M_{H_2}^2 c_\alpha^2 \end{pmatrix} \equiv \mathcal{M}. \quad (2.3)$$

The mixing angle α is determined by

$$\tan 2\alpha = \frac{2\mathcal{M}_{12}}{\mathcal{M}_{22} - \mathcal{M}_{11}}, \text{ or } \sin 2\alpha = \frac{2\lambda_{H\Phi} v_H v_\Phi}{M_{H_2}^2 - M_{H_1}^2}.$$

This renormalizable model Eq. (2.1) has four more parameters compared with the SM: λ_Φ , v_{v_Φ} , g_X and $\lambda_{H\Phi}$. For convenience, we shall use the following set as input parameter, M_X , M_{H_2} , g_X and $\sin \alpha$. Since our aim is to explain the positron excess observed by PAMELA and AMS02 with VDMs, we will concentrate mainly on heavy VDM with mass around a few TeV in this paper.

III. $\mathcal{O}(\text{TeV})$ VDM AND PHENOMENOLOGICAL CONSTRAINTS

For successful explanation of the positron excess reported by PAMELA and AMS02, we need a dark matter around $\mathcal{O}(\text{TeV})$. Therefore we first would like to show that such a heavy VDM can still be compatible with other constraints from collider, relic density, theoretical consistencies, *etc.*. Figs. 2, 3 and Fig. 5 show that there is an ample parameter space for accommodating a TeV VDM. In this section, we shall provide detailed discussions on various relevant constraints on the renormalizable model Lagrangian Eq. (2.1) one by one. The indirect signature from the renormalizable model and from higher dimensional operators will be discussed in Sec. IV and Sec. V, respectively.

A. Constraint from Higgs data

The current Higgs data gives constraint on the mixing angle, $|\sin \alpha| \lesssim 0.32$ or $\sin^2 \alpha \lesssim 0.1$ [41]. In the Fig. 2, the region above the horizontal dot-dashed line has $\sin \alpha > 0.32$ and therefore is disfavored by the current LHC data on the Higgs signal strengths in various production and decay channels. Then we can make an approximation:

$$\cos \alpha \simeq 1, \text{ and } \sin \alpha \simeq \frac{\lambda_{H\Phi} v_H v_\Phi}{M_{H_2}^2 - M_{H_1}^2}.$$

When $M_X \sim 2 \text{ TeV}$, the relic density constrains the gauge coupling to be $g_X \sim 0.7$, as shown in Fig. 2. If we further assume that H_2 is still in thermal equilibrium before the VDMs (X_μ 's) freeze out, its mass should be smaller than M_X . Taking $M_{H_2} \sim 500 \text{ GeV}$

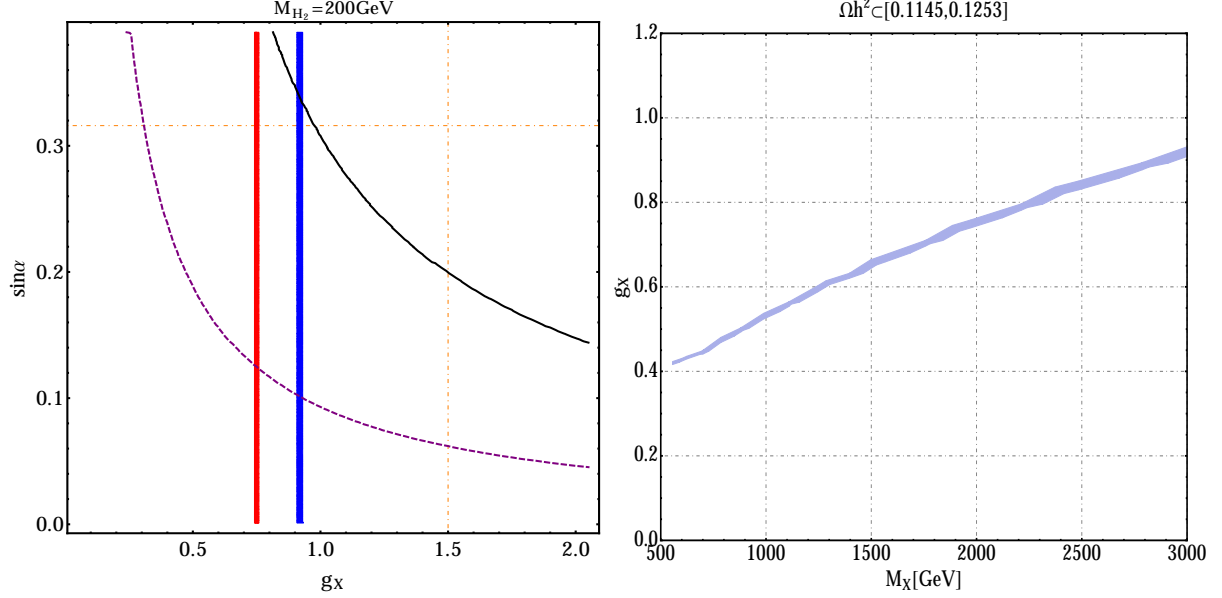


FIG. 2: (Left panel) The horizontal dot-dashed line sets the boundary for $\sin \alpha \simeq 0.32$ or $\sin^2 \alpha \simeq 0.1$ from Higgs data. The vertical dot-dashed one marks the limit for perturbativity. The solid (dashed) curves correspond to $\sigma_{\chi N} = 10^{-44}$ (10^{-45}) cm². The vertical red and blue bands set the correct relic density for $M_X = 2$ TeV, 3 TeV, respectively. (Right panel) This plot shows the relation between g_X and M_X constrained by Ωh^2 , the blue band region is allowed with 2σ variation.

and tiny mixing for example, we have

$$\begin{aligned}\lambda_{H\Phi} &\sim \frac{\sin \alpha (500^2 - 125^2)}{246 \times 2000} \sim 0.5 \times \sin \alpha, \\ \lambda_\Phi &\sim \frac{500^2}{2 \times 2000^2} = 0.03, \\ \lambda_H &= \frac{125^2 + (500^2 - 125^2) \sin^2 \alpha}{2 \times 246^2} \simeq 0.13 + 2 \sin^2 \alpha.\end{aligned}$$

This only gives an estimation of approximate values for the parameters. Throughout this section, we restrict the parameters

$$M_X \gtrsim \text{TeV}, M_{H_2} \lesssim \text{TeV}, g_X \lesssim 1.5, \sin^2 \alpha \lesssim 0.1. \quad (3.1)$$

The viable and exact values of M_X and g_X are further constrained by thermal relic density and perturbativity as discussed below. Distributions of these viable points are illustrated in Figs. 2, 3, 5 and 6.

The mixing angle α is also constrained by dark matter direct search and the lifetime of H_2 as shown in the right plot of Fig. 5. The upper bound is from XENON100 [42] (yellow), LUX [43] (orange), and vacuum stability (blue) for 2 TeV VDM as an example, inside the yellow and orange regions are excluded. The EW vacuum becomes absolutely stable in the blue region. The lower bound comes from the BBN constraint on the lifetime of H_2 where we require $\tau_{H_2} < 10^{-2}$ s, since a long-lived H_2 could be dangerous to the successful BBN if $\sin \alpha$ is very small. It turns out that thermalization of the dark sector puts a much more stringent lower bound than BBN except in the low M_{H_2} region. We shall discuss this later in detail.

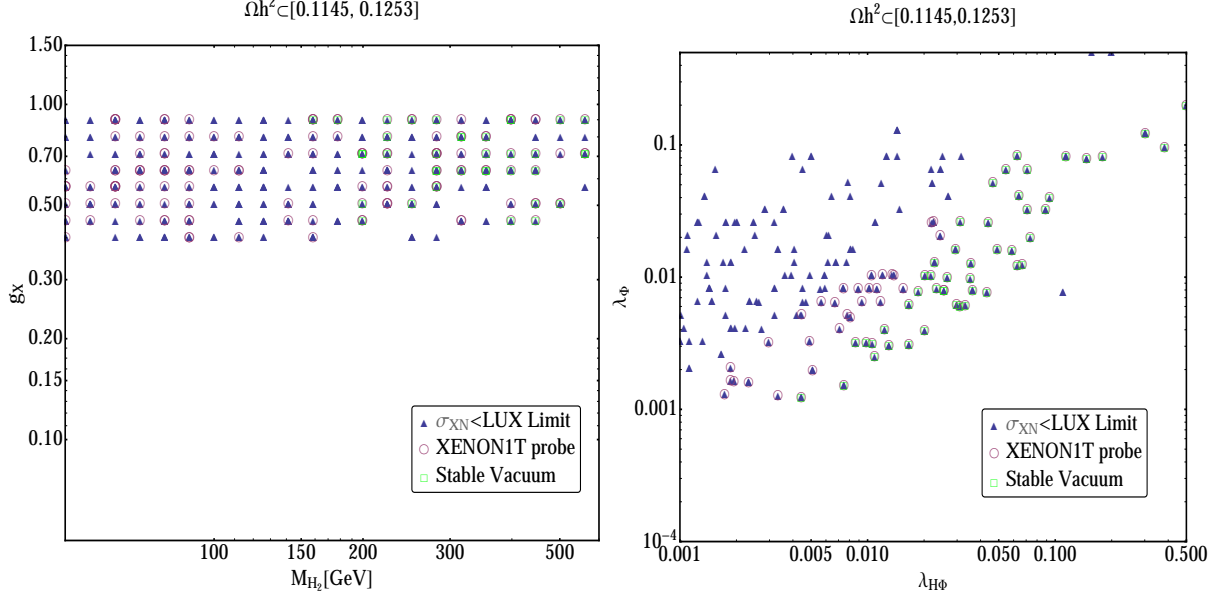


FIG. 3: Scatter plots with different axis for $M_X \sim \mathcal{O}(\text{TeV})$. Every point satisfies the relic density in 2σ . Blue triangles are below the LUX Limit and purple circles can be probed by dark matter direct search in the near future. Green squares give stable EW vacuum. It can be seen that all green squares can be probed by the XENON1T.

B. Thermal relic density

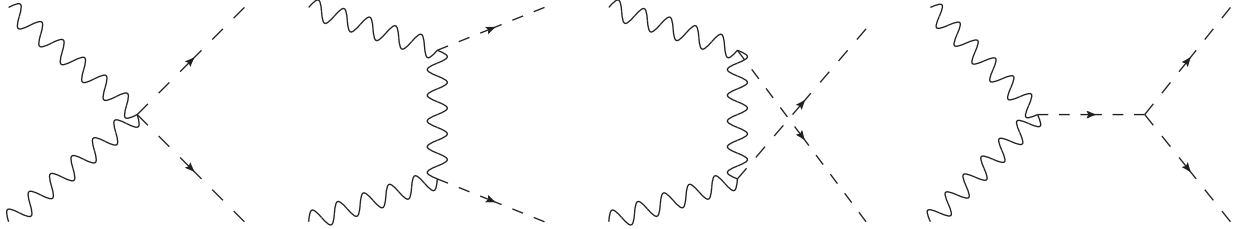


FIG. 4: Feynman diagrams. The last one can be neglected due to the smallness of λ_Φ .

We are interested in the parameter space, $M_X \sim \mathcal{O}(1)$ TeV and $M_{H_2} \sim \mathcal{O}(100)$ GeV, aiming at explaining the positron excess. As a result, λ_Φ and $\lambda_{H\Phi}$ are small enough that only the first three feynman diagrams of Fig. 4 need to be considered for X_μ annihilation. For heavy X_μ and small mixing between H_1 and H_2 , $XX \rightarrow H_2 H_2$ is the dominant annihilation channel. σv is then calculated as

$$\begin{aligned} \sigma v &= \frac{1}{3 \times 3 \times 2} \frac{1}{2 M_X \sqrt{s}} \int \frac{|\mathcal{M}|^2 |p_1|}{(4\pi)^2 \sqrt{s}} d\Omega \\ &\simeq \frac{g_X^4}{144\pi M_X^2} \left[3 - \frac{8(M_{H_2}^2 - 4M_X^2)}{M_{H_2}^2 - 2M_X^2} + \frac{16(M_{H_2}^4 - 4M_{H_2}^2 M_X^2 + 6M_X^4)}{(M_{H_2}^2 - 2M_X^2)^2} \right], \end{aligned} \quad (3.2)$$

where $\frac{1}{3 \times 3 \times 2}$ accounts for the averaging over polarizations for initial states and identical

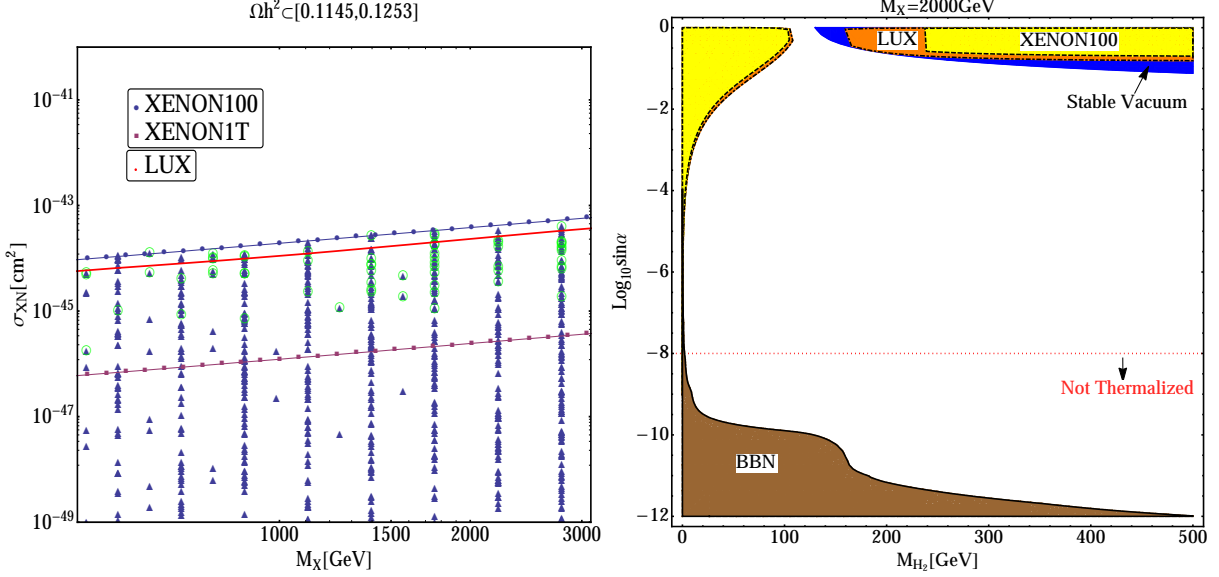


FIG. 5: The left panel shows the scatter plot with direct search constraints from the latest XENON100 [42], LUX[43](red line) and the future XENON1T as function as the dark matter mass and green squares give stable EW vacuum. It can be seen that all green squares can be probed by the XENON1T. The right panel shows the constraints on the mixing angle α . The upper bound is from XENON100(yellow), LUX(orange) and vacuum stability(blue), and the lower bound comes from the BBN constraint on the lifetime and thermalization of H_2 .

factor for final states, $s \simeq 4M_X^2$ at decoupling time, and

$$|\mathcal{M}|^2 = g_X^4 \left[12 - \frac{32(M_{H_2}^2 - 4M_X^2)}{M_{H_2}^2 - 2M_X^2} + \frac{64(M_{H_2}^4 - 4M_{H_2}^2 M_X^2 + 6M_X^4)}{(M_{H_2}^2 - 2M_X^2)^2} \right].$$

Since at the leading approximation σv is independent of v , we can replace the thermal averaged $\langle \sigma v \rangle$ with Eq. (3.2) in the calculation of relic density. For $\langle \sigma v \rangle \sim 3 \times 10^{-26} \text{cm}^3 \text{s}^{-1}$, $M_X \sim \text{TeV}$ and $M_{H_2} \ll M_X$, we have

$$g_X \sim 0.57 \times \left(\frac{M_X}{1 \text{TeV}} \right)^{\frac{1}{2}}. \quad (3.3)$$

As shown in Fig. 2, the red and blue vertical band display the correct relic density ($\Omega h^2 = 0.1199 \pm 0.0027$ [1]) of dark matter for $M_X = 2 \text{ TeV}$ and $M_X = 3 \text{ TeV}$, respectively. The precise relation between g_X and M_X is shown in the right panel of Fig. 2, where we used `micrOMEGAs3.1` [44] for the numerical calculation.

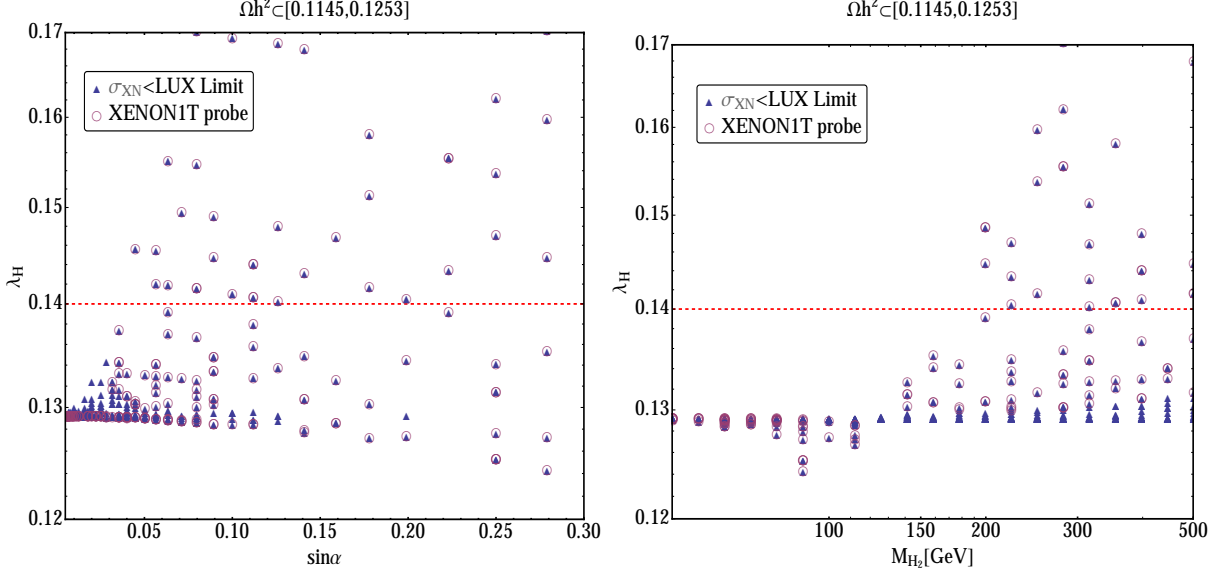


FIG. 6: Scatter plots show the Higgs quartic coupling λ_H with different x-axis for $M_X \sim \mathcal{O}(\text{TeV})$. Every point satisfies the relic density in 2σ . Blue triangles are below the LUX Limit and purple circles can be probed by dark matter direct search in the near future. Regions above the horizontal red dotted line give stable EW vacuum.

C. Perturbativity and Vacuum Stability

Perturbativity and vacuum stability of the model can be determined by running RGEs [12] to higher energy scales:

$$\begin{aligned} \frac{d\lambda_H}{d\ln\mu} &= \frac{1}{16\pi^2} \left[24\lambda_H^2 + \lambda_{H\Phi}^2 - 6y_t^4 + \frac{3}{8} \left(2g_2^2 + (g_1^2 + g_2^2)^2 \right) - \lambda_H (9g_2^2 + 3g_1^2 - 12y_t^2) \right], \\ \frac{d\lambda_{H\Phi}}{d\ln\mu} &= \frac{1}{16\pi^2} \left[2\lambda_{H\Phi} (6\lambda_H + 4\lambda_\Phi + 2\lambda_{H\Phi}) - \lambda_{H\Phi} \left(\frac{9}{2}g_2^2 + \frac{3}{2}g_1^2 - 6y_t^2 + 6g_X^2 \right) \right], \\ \frac{d\lambda_\Phi}{d\ln\mu} &= \frac{1}{16\pi^2} \left[2(\lambda_{H\Phi}^2 + 10\lambda_\Phi^2 + 3g_X^4) - 12\lambda_\Phi g_X^2 \right], \\ \frac{dg_X}{d\ln\mu} &= \frac{1}{16\pi^2} \frac{1}{3} g_X^3. \end{aligned}$$

For small λ_Φ and $\lambda_{H\Phi}$, the dark sector has negligible effects on the RG running of λ_H . Similarly to the SM, due to the top quark's negative contribution from large Yukawa coupling y_t , λ_H is running negative at high scale M_Λ , leading to a metastable electroweak vacuum whose lifetime is longer than the age of our Universe. Although the precise M_Λ depends sensitively on y_t and strong coupling constant, using their central values and positivity of λ_H at scales larger than 10^{15}GeV would require $\lambda_H \gtrsim 0.14$ at the weak scale. This would put a constraint on M_{H_2} and $\sin\alpha$ from [12]

$$\lambda_H = \frac{M_{H_1}^2 \cos^2 \alpha + M_{H_2}^2 \sin^2 \alpha}{2v_H^2} \gtrsim 0.14. \quad (3.4)$$

The allowed parameter space is shown as the blue region in the right panel of Fig. 5 and electroweak vacuum is metastable outside of the region. We also show scatter plots for λ_H

vs. $\sin \alpha$ and λ_H vs. M_{H_2} in Fig. 6, sizable deviation from the SM value is possible within current limits on $\sin \alpha$, thermal relic density and direct search for X_μ . Since the deviation can be as large as $\mathcal{O}(10\%)$ at tree level, it might be probed at future colliders, such as the ILC for instance. Moreover, all points giving stable vacuum can be tested at XENON1T, as we shall discuss in the following subsection.

The perturbative limit is set by the input value of g_X . We find that $g_X \lesssim 1.6(1.5)$ can give perturbative theory up to M_{GUT} (Planck scale), respectively. Correspondingly, the mass of dark matter is bounded from above, $M_X \simeq 7$ TeV for $g_X \simeq 1.5$ from Eq. (3.3) if non-perturbative effect is neglected.

D. Direct search

The VDM X_μ can interact with a nucleus through the mixing of h and φ . The cross section of X_μ 's scattering off a nucleon is given by

$$\sigma(X_\mu N \rightarrow X_\mu N) = \frac{1}{16\pi} g_X^4 \sin^2 2\alpha \frac{f^2 m_N^2}{v_H^2} \left(\frac{1}{m_{H_2}^2} - \frac{1}{m_{H_1}^2} \right)^2 \left(\frac{M_X m_N}{M_X + m_N} \right)^2.$$

Note that there is a generic cancellation between the H_1 and H_2 contributions [12]. When $M_X \gg m_N$, $\frac{M_X m_N}{M_X + m_N} \simeq m_N$, direct dark matter search experiments will only constrain the product $g_X^4 \sin^2 2\alpha$, independent of M_X . In the Fig. 2, we show the contours for $\sigma_{XN} \equiv \sigma(X_\mu N \rightarrow X_\mu N)$. The solid(dashed) curve corresponds $\sigma_{XN} = 10^{-44} (10^{-45}) \text{cm}^2$, region on the right-handed side gives larger σ_{XN} . Note that for large M_X the XENON100's bounds [42] are around $2 \times (\frac{M_X}{1 \text{TeV}}) \times 10^{-44} \text{cm}^2$ and LUX [43] improved the limit by a factor of 2.

In Figs. 3,5,6, we show the scatter plots for the relevant parameters which satisfy the constraints from relic density and LUX and can be probed by the near future XENON1T experiment. We can see that most parameter space except $M_{H_2} \simeq M_{H_1}$ where the cancellation occurs or no-mixing, $\sin \alpha \simeq 0$, can be covered by XENON1T. If we require the electroweak vacuum is stable up to high energy scale, then all the allowed points are covered by XENON1T. This is explicitly shown as green squares in Fig. 3 and green circles in Fig. 5.

E. Thermalization of X_μ and H_2

When calculating thermal relic density of VDMs, we are implicitly assuming X_μ still has the same temperature as the thermal bath before its freezing out. This is justified as long as H_2 is in equilibrium³ since X_μ is thermalized by X_μ - H_2 interaction. In general, all related processes, such as scattering one $H_2 + Y \leftrightarrow H_2 + Y$ (Y is any other particle in the thermal bath), may have to be considered. As an illustration, in the limit of a tiny mixing angle α , we consider one channel for thermalizing H_2 , $H_2 H_2 \leftrightarrow H_1 H_1$, which is the most efficient one for thermalization when the temperature is high. We then have the approximate relations:

$$\Gamma \simeq n_{H_2} \times \langle \sigma v \rangle_{H_2 H_2 \leftrightarrow H_1 H_1}, \quad n_{H_2} \sim T^3, \quad \langle \sigma v \rangle \sim \frac{\lambda_{H\Phi}^2}{T^2},$$

³ We require H_2 is in chemical equilibrium since kinetic decoupling occurs much later and give less stringent constraints.

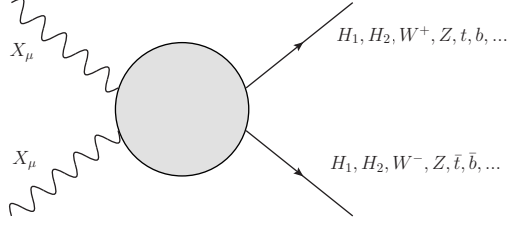


FIG. 7: annihilation process.

In the radiation dominated era, the Hubble constant is $H \sim T^2/M_{pl}$, so the condition for equilibrium gives

$$\Gamma \gtrsim H \Rightarrow \lambda_{H\Phi}^2 \gtrsim \frac{T}{M_{pl}}.$$

For $T \simeq 1\text{TeV}$ we have $|\lambda_{H\Phi}| \gtrsim 10^{-8}$, which in turn leads to $\sin \alpha \gtrsim 10^{-8}$. As shown in the right panel of Fig. 5, region under the red dotted line means the dark sector is not thermalized and this constraint is much more stringent than BBN constraint except in the low M_{H_2} region. The only purpose of the above discussion is to show that even for very tiny $\lambda_{H\Phi}$, H_2 is still in thermal equilibrium when X_μ starts freezing out.

IV. INDIRECT SIGNATURES FROM VDM PAIR ANNIHILATION

Most phenomenology of the VDM with mass $\mathcal{O}(100\text{GeV})$ has been studied in Ref. [12], except for its indirect signatures. In this section, we focus on the indirect signatures from the pair annihilation of VDMs (as shown in Fig. 7) which are described by the renormalizable model Lagrangian, Eq. (2.1). Depending on the parameters, the dominant annihilation channels can be different, which results in different spectra for cosmic rays.

Since it is impractical to show all the cases, here we only discuss several typical ones, as tabulated in Table I. For a TeV VDM (X_μ), the reaction $X_\mu X_\mu \rightarrow H_2 H_2$ is the dominant annihilation channel. Therefore the spectrum shape will be truncated at M_X , and fully determined by H_2 's decay modes. The lighter X_μ cases, C and D, are chosen just for completeness and comparison with case A and B. All these cases are still allowed by current experimental constraints considered in the previous section, giving the correct thermal relic density of the VDM, although the dominant annihilation channels for indirect detection for each case could be different from each other. Note that case B would not give an absolute stable vacuum but a metastable vacuum, and here we choose this low M_{H_2} case just for comparison.

The production rate for cosmic ray from dark matter annihilation is given by [45]

$$Q(E, \vec{r}) = \frac{1}{2} \left(\frac{\rho(\vec{r})}{M_{\text{DM}}} \right)^2 \sum_i \langle \sigma v \rangle_i \frac{dN_i}{dE}. \quad (4.1)$$

$\frac{dN_i}{dE}$ is the energy spectrum function from a specific annihilation channel i , and $M_{\text{DM}} = M_X$ in our discussion. The function $\rho(r)$ is the density profile of dark matter. We shall use the Navarro-Frenk-White (NFW) density profile [46],

$$\rho(\vec{r}) = \rho_\odot \left[\frac{r_\odot}{r} \right] \left[\frac{1 + (r_\odot/r_c)}{1 + (r/r_c)} \right]^2.$$

–	$M_X[\text{GeV}]$	$M_{H_2}[\text{GeV}]$	g_X	$\sin \alpha$	$\langle \sigma v \rangle [10^{-26} \text{cm}^3/\text{s}]$	$\sigma_{XN} [10^{-45} \text{cm}^2]$
case A	1100	280	0.56	0.08	2.25	0.77
case B	1100	90	0.56	0.05	2.36	0.40
case C	400	500	0.34	0.30	2.32	2.68
case D	400	250	0.37	0.14	2.35	0.46

TABLE I: Four cases for illustrating indirect signatures, all are still allowed by current experimental constraints.

Here we use $\rho_\odot \simeq 0.3 \text{GeV}/\text{cm}^3$, $r_\odot \simeq 8.5 \text{kpc}$ and $r_c \simeq 20 \text{kpc}$. After production, charged particles propagate through the Galaxy and lose their energy before reaching the solar system. Then the number density $\psi(E, r_\odot)$ can be expressed as [44]

$$\psi(E, \vec{r}_\odot) = \int_E^{M_X} dE' \int d^3\vec{r} G(\vec{r}_\odot, E; \vec{r}, E') Q(E', \vec{r}),$$

where $G(\vec{r}_\odot, E; \vec{r}, E')$ is the Green's function, parametrizing the effect during the propagation, such as diffusion and energy loss. Finally the flux is given by

$$\Phi = \frac{v(E)}{4\pi} \psi.$$

For γ -ray and neutrinos, after production they travel almost freely, so the fluxes are only dependent on the integral of the squared ρ over the line of sight

$$\Phi_{\gamma/\nu} \propto \int_0^\infty dr \rho^2(r'),$$

where $r' = \sqrt{r^2 + r_\odot^2 - 2rr_\odot \cos \theta}$ and θ is the angle in the direction of observation. We shall use $\theta = \pi/6$ as an example and neglect the γ -ray induced by inverse Compton scattering and synchrotron radiation from the primary e^+ and \bar{p} for simplicity. This is justified as long as we concentrate on the high energy part of the spectrum from $10^{-2}M_X$ to M_X . Relative sizes of various contributions are illustrated in [47].

Generally, the VDM mass determines the energy cut-off of the primary spectra. Since H_2 couples to the SM particles with the same pattern as that of H_1 , its mass determines the branching ratios completely. These different decay final products, together with relevant importance of annihilation channels, can lead different spectra for cosmic rays, as shown in Fig. 8, although all of them have similar size of $\langle \sigma v \rangle$.

For instance in e^+ spectrum, in case C, the dominant annihilation channel is $X_\mu + X_\mu \rightarrow W^+ + W^-$, while $X_\mu + X_\mu \rightarrow H_2 + H_2$ is the dominant one for case D. About 1/3 of W decay directly to charged leptons and the rest decay hadronically, in sum for charged particles the multiplicity is about 20 in a single W decay. While a 250GeV H_2 mostly decays to ZZ and W^+W^- whose decay products are then boosted differently. This is the main reason responsible for the different spectra in case C and D. Similar mechanisms apply to other spectra for γ , \bar{p} and ν 's. For the overall differences between case A/B and case C/D, although the primary spectra dN/dE in case A and B are larger than those in case C and D, the fluxes at earth have the opposite behavior in some energy ranges. This is mainly due to the factor $(\rho/M_{\text{DM}})^2$ in the source function Q , Eq. 4.1, and lighter dark matter tends to have larger Φ in the kinematics-allowed energy range.

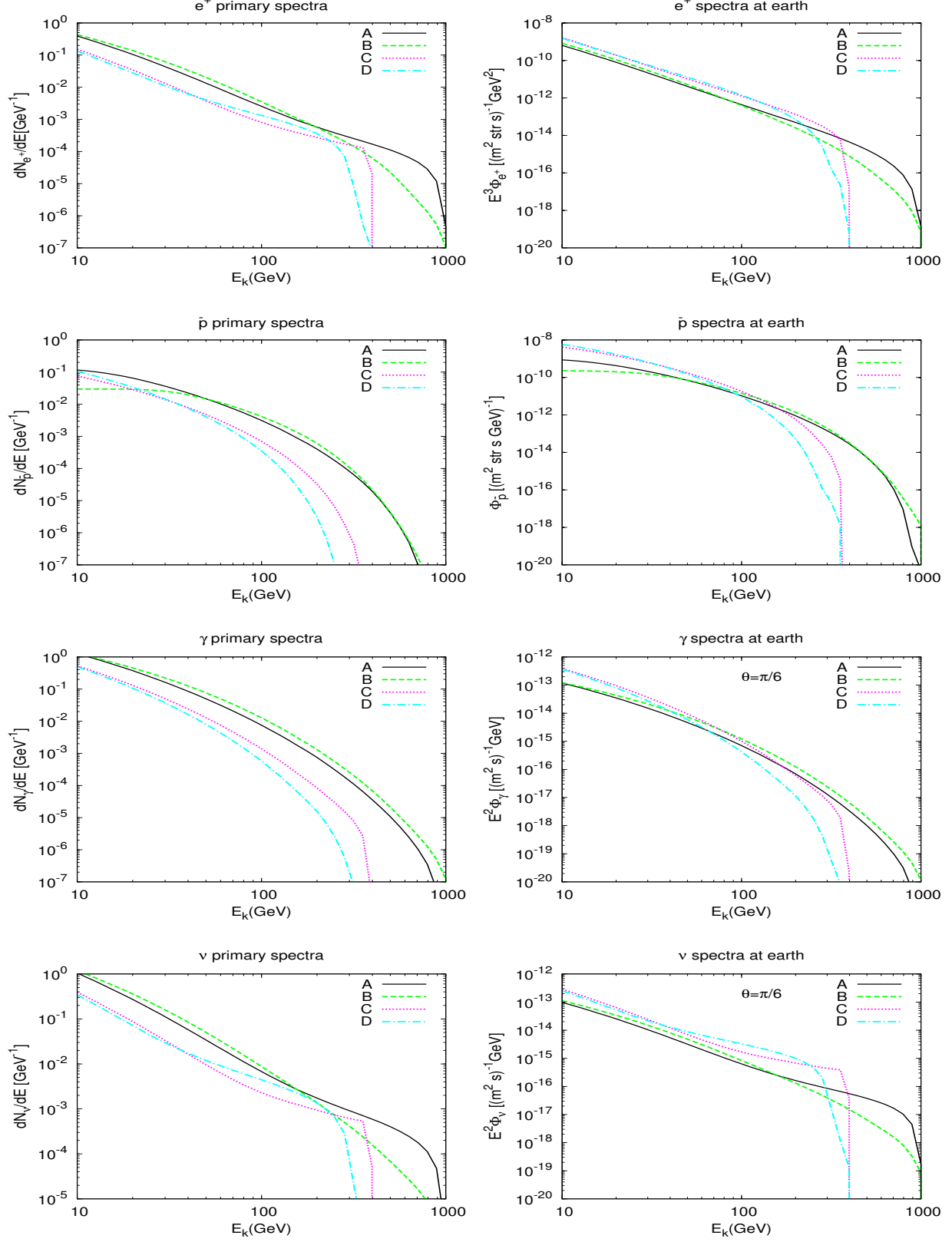


FIG. 8: Spectra of e^+ , \bar{p} , γ and ν from vector dark matter annihilation only. The left panels show the primary spectra while the right ones show the spectra at earth after propagation (the units are chosen with the usual convention).

Note that the spectra we discussed so far are only the signatures from dark matter, and in reality astrophysical observations of cosmic rays and γ -ray are the sum of the much larger backgrounds and the above signals. For canonical values of thermal $\langle\sigma v\rangle$, the differences among those cases can hardly be distinguished unless there are some mechanisms for boosting the spectrum, such as Sommerfeld enhancement [48, 49] and Breit-Wigner resonance [50–52] enhancement for explaining the recent observed positron excesses in [13–15]. However, stringent constraints from CMB have been put on such mechanisms for annihilating dark matter [53, 54]. Therefore we conclude that the VDM pair annihilations from the renormalizable Lagrangian (2.1) cannot account for the positron excess observed by PAMELA and AMS02. And we shall focus on the decaying dark matter scenario in the next section.

V. INDIRECT SIGNATURES FROM VDM (X_μ) DECAY

A. Effective Operators for decaying VDM (X_μ)

In the renormalizable theory described by the Lagrangian (2.1), the dark matter X_μ can not decay because of the Z_2 symmetry we assumed. This is not true any more if higher dimensional nonrenormalizable operators are taken into account. Generally, higher dimensional operators are suppressed by the power of some new physics scale Λ , above which the nonrenormalizable Lagrangian begins to violate unitarity and fails to describe physical phenomena correctly. In the absence of a complete theory above Λ , we may write down all the operators which are invariant under the gauge group $G_{SM} \times U(1)_X$. To which orders we shall truncate is dependent on the observable we are considering. In the following, we only list higher dimensional operators up to dimension-6, especially we focus on those involving both fields from the dark sector and from the SM sector. Such higher dimensional operators for SM sector upto dim-6 can be found in Ref.s [55, 56].

Since there are two fields, Φ and X^μ , in the dark sector, gauge invariant operators in the dark sector would be made of the following operators:

$$\Phi^\dagger\Phi, \Phi^\dagger i \overleftrightarrow{D}_\mu\Phi, X^{\mu\nu}, \tilde{X}^{\mu\nu}.$$

where $\Phi^\dagger \overleftrightarrow{D}_\mu\Phi = \Phi^\dagger D_\mu\Phi - (D_\mu\Phi)^\dagger\Phi$. The independent effective operators of dimension 6 in this sector are

$$(\Phi^\dagger\Phi)^3, (\Phi^\dagger\Phi)\Box(\Phi^\dagger\Phi), (\Phi^\dagger D^\mu\Phi)^\dagger(\Phi^\dagger D^\mu\Phi), \Phi^\dagger\Phi X_{\mu\nu}X^{\mu\nu}, \Phi^\dagger\Phi\tilde{X}_{\mu\nu}X^{\mu\nu}.$$

$(D_\mu\Phi)^\dagger(D_\nu\Phi)X^{\mu\nu}$ is redundant, it can be shown by partial integration and using equations of motion. Gauge invariant operators in SM sector are products of the following basis,

$$H^\dagger H, H^\dagger i \overleftrightarrow{D}_\mu H, B^{\mu\nu}, \tilde{B}^{\mu\nu}, \bar{L}_i R_j H, \bar{f}_i \gamma^\mu f_j, (\bar{L}_i \sigma^{\mu\nu} R_j) H, H^\dagger \tau^I H W_{\mu\nu}^I, H^\dagger \tau^I H \tilde{W}_{\mu\nu}^I,$$

where L and R stand for left-handed and right-handed fermion fields, respectively. Note that there is only one dimension-five operator, the Weinberg operator for Majorana neutrino mass.

Dimension-6 operators that involve both SM and dark sector fields are

$$\begin{aligned}
& (\Phi^\dagger \Phi)^2 H^\dagger H, \Phi^\dagger \Phi (H^\dagger H)^2, \Phi^\dagger \Phi \square H^\dagger H, \left(\Phi^\dagger i \overleftrightarrow{D}_\mu \Phi \right) \left(H^\dagger i \overleftrightarrow{D}_\mu H \right), \\
& \Phi^\dagger \Phi \left(\bar{L}_i R_j H + h.c. \right), \left(\Phi^\dagger i \overleftrightarrow{D}_\mu \Phi \right) \left(\bar{L}_i \gamma^\mu L_j + \bar{R}_i \gamma^\mu R_j \right), \left(\bar{L}_i \sigma^{\mu\nu} R_j \right) H X^{\mu\nu} + h.c., \\
& \Phi^\dagger \Phi B_{\mu\nu} X^{\mu\nu}, \Phi^\dagger \Phi \tilde{B}_{\mu\nu} X^{\mu\nu}, H^\dagger H B_{\mu\nu} X^{\mu\nu}, H^\dagger H \tilde{B}_{\mu\nu} X^{\mu\nu}, H^\dagger H X_{\mu\nu} X^{\mu\nu}, H^\dagger H \tilde{X}_{\mu\nu} X^{\mu\nu}, \\
& H^\dagger \tau^I H W_{\mu\nu}^I X^{\mu\nu}, H^\dagger \tau^I H \tilde{W}_{\mu\nu}^I X^{\mu\nu}.
\end{aligned}$$

The above operators make the whole independent set of operators with both the SM fields and the dark sector fields. Others can be reduced to linear combinations of these operators by using equations of motion.

After the symmetry breaking of $G_{SM} \times U(1)_X$, some of the above effective operators can lead to dark matter X_μ decay. Let us consider operators for the VDM decays into two SM particles in the final state:

$$\begin{aligned}
1. \quad & \left(\Phi^\dagger i \overleftrightarrow{D}_\mu \Phi \right) \left(H^\dagger i \overleftrightarrow{D}^\mu H \right) \Rightarrow X^\mu \rightarrow \varphi/h + \gamma/Z, \\
2. \quad & \left(\Phi^\dagger i \overleftrightarrow{D}_\mu \Phi \right) (\bar{f} \gamma^\mu f), \bar{L} \sigma_{\mu\nu} R H X^{\mu\nu} + h.c. \Rightarrow X^\mu \rightarrow \bar{f} + f, \\
3. \quad & \Phi^\dagger \Phi B_{\mu\nu} X^{\mu\nu}, \Phi^\dagger \Phi \tilde{B}_{\mu\nu} X^{\mu\nu}, (\Phi \rightarrow H) \Rightarrow X^\mu \rightarrow \varphi/h + \gamma/Z, \\
4. \quad & H^\dagger \tau^I H W_{\mu\nu}^I X^{\mu\nu}, H^\dagger \tau^I H \tilde{W}_{\mu\nu}^I X^{\mu\nu} \Rightarrow X^\mu \rightarrow \varphi/h + \gamma/Z,
\end{aligned}$$

There are also some interesting three-body decay channels, such as

$$\Phi^\dagger \Phi B_{\mu\nu} X^{\mu\nu} \Rightarrow X^\mu \rightarrow \varphi + \varphi + \gamma/Z.$$

Generally, three-body decays from these operators are more suppressed compared with two-body decay because of the smaller phase space available. Therefore we will mainly discuss the two-body decay in the following.

B. A simple UV completion

It should be pointed out that not all of the above operators need to be investigated simultaneously for the purpose of the positron excess observed by PAMELA and AMS02. The choice is highly dependent on the exact theory beyond energy scale Λ and low energy observables we are interested in. For instance, Refs. [57, 58] investigated γ -ray in a similar framework. Here as a concrete illustration for fermionic final states, let us consider the following operator

$$\left(\Phi^\dagger i \overleftrightarrow{D}_\mu \Phi \right) (\bar{f} \gamma^\mu f),$$

it can induce such a decay channel,

$$X^\mu \rightarrow f \bar{f}.$$

This operator can be induced from the following interactions when both Φ and f are charged under a new extra $U(1)'$ symmetry with A'_μ gauge field,

$$\mathcal{L} = (D'_\mu \Phi)^\dagger D'^\mu \Phi + \bar{f} i \gamma^\mu D'_\mu f - \frac{1}{4} F'^{\mu\nu} F'_{\mu\nu} + (D'_\mu \phi)^\dagger D'^\mu \phi - V(\phi^\dagger \phi),$$

where the covariant derivatives are

$$\begin{aligned} D'_\mu \Phi &= (\partial_\mu + ig_X Q_X X_\mu + ig' Q'_\Phi A'_\mu) \Phi, \\ D'_\mu \phi &= (\partial_\mu + ig' Q'_\phi A'_\mu) \phi, \\ D'_\mu f &= (D_\mu^{\text{SM}} + ig' Q'_f A'_\mu) f. \end{aligned}$$

A new scalar ϕ has been introduced in order to break $U(1)'$ spontaneously and make A'_μ massive. If only leptons have $U(1)'$ charges among the SM particles, then the massive VDM X^μ would decay to a lepton pairs only,

$$X^\mu \rightarrow l^+ l^-, \quad l = e, \mu, \tau.$$

In such a case, $U(1)'$ charge can be identified as lepton number ⁴, and ϕ could also couple to right-handed neutrino and give the Majorana mass term after $U(1)'$ breaking, acting as the source of type-I seesaw mechanism. If only e^\pm and ν_R are $U(1)'$ -charged, then X_μ only decays to $e^+ e^-$, see refs.[17, 59] for similar models. For simplicity, we shall assume 100% of X_μ decay to a single channel for indirect signatures.

In order to explain the positron excess correctly, the lifetime of dark matter should be around $\tau_{DM} \sim 10^{26}$ s, which determines the scale Λ ,

$$\Gamma \sim \frac{g_\Lambda^4 M^5}{\Lambda^4}, \quad \tau = \frac{\hbar}{\Gamma} \sim 10^{26} \text{s} \Rightarrow \Gamma \sim 6 \times 10^{-51} \text{GeV}.$$

For $M = 1 \text{TeV}$, we have

$$\Lambda \sim g_\Lambda \left(\frac{M^5 \tau}{\hbar} \right)^{\frac{1}{4}} = g_\Lambda \left(\frac{10^{15} \text{GeV}^5 \times 10^{26} \text{s}}{6.583 \times 10^{-25} \text{GeV s}} \right)^{\frac{1}{4}} \sim 2g_\Lambda \times 10^{16} \text{GeV},$$

If $g_\Lambda \sim 0.1$ then $\Lambda \sim 2 \times 10^{15} \text{GeV}$. In the framework of the above $U(1)'$ model, we have the following identifications: $\Lambda \rightarrow M_{A'}$, $g_\Lambda \rightarrow g'$ and $M^5 \rightarrow M_X^3 v_\Phi^2$.

C. Decaying VDM (X_μ) and positron excesses

Discussions in the subsection are not entirely new and a number of delicate model-independent analysis exist in the literature [16, 17, 19, 20, 23, 25–28, 30, 33, 35]. Here we focus on the $X_\mu \rightarrow l^+ l^-$, $l = (e, \mu, \tau)$, and shall give detailed explanation on why each channel can or cannot fit the data.

Since we assume X_μ can decay to leptons only, it will give rise to indirect signatures in cosmic e^\pm , which can be conveniently discussed in terms of two observables: the total flux $\Phi_{e^-+e^+}$ and the positron fraction $\Phi_{e^+}/\Phi_{e^-+e^+}$. Each Φ is the sum of background flux and the contribution from dark matter decay. The e^\pm background fluxes of interstellar origin can be analytically parametrized as [14, 47]

$$\begin{aligned} \Phi_{e^-}^{\text{bkg}}(E) &= \left(\frac{82.0 \times E^{-0.28}}{1 + 0.224 \times E^{2.93}} \right) \text{GeV}^{-1} \text{m}^{-2} \text{s}^{-1} \text{sr}^{-1}, \\ \Phi_{e^+}^{\text{bkg}}(E) &= \left(\frac{38.4 \times E^{-4.78}}{1 + 0.0002 \times E^{5.63}} + 24.0 \times E^{-3.41} \right) \text{GeV}^{-1} \text{m}^{-2} \text{s}^{-1} \text{sr}^{-1}, \end{aligned}$$

⁴ We ignore the anomaly cancellation issue in this paper.

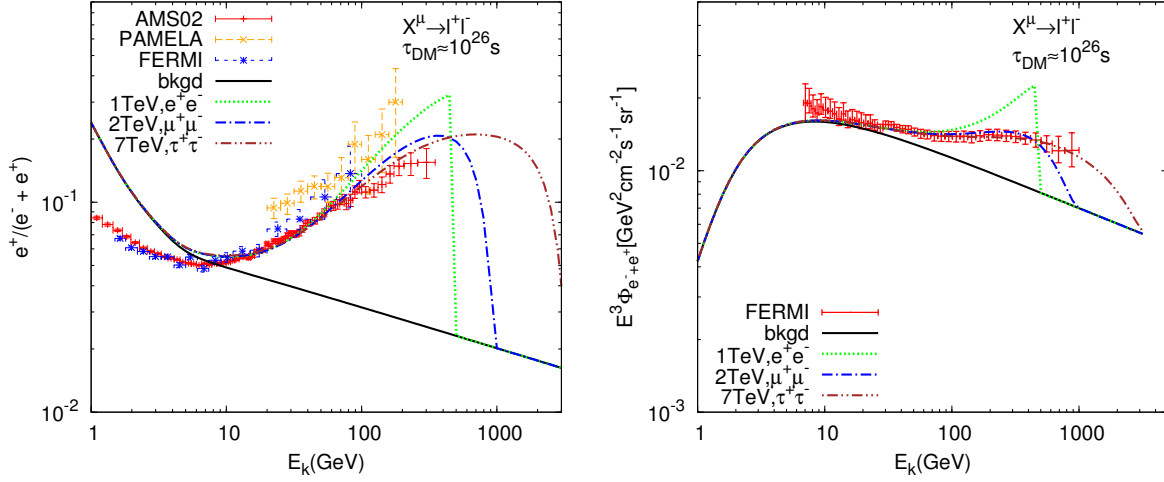


FIG. 9: These figures show the spectra of the e^+ fraction and e^\pm total flux from the decay, $X^\mu \rightarrow l^+ l^-$, $l = e, \mu, \tau$ and lifetime τ_{DM} is chosen to $(4, 2, 0.7) \times 10^{26}$ s, respectively. See details in text.

where E is in GeV unit. For the flux from vector dark matter decay, we calculate it with modifying `micrOMEGAs`[44]. The production rate is given by

$$Q(E, \vec{r}) = \frac{\rho(\vec{r})}{M_{\text{DM}} \tau_{\text{DM}}} \frac{dN^{e^\pm}}{dE}, \quad (5.1)$$

dN^{e^\pm}/dE is the energy spectrum function, $M_{\text{DM}} = M_X$ in our discussion, τ_{DM} is the lifetime of X_μ and $\rho(r)$ is the density profile of dark matter. We use the NFW profile for the decaying DM, too.

In Fig. 9, we show the spectra of the positron fraction and $\Phi_{e^-+e^+}$ for individual decay channel, $X^\mu \rightarrow l^+ l^-$, $l = e, \mu, \tau$. To compare with experimental observation, we have also shown the data from PAMELA, Fermi and AMS02. In the low energy range $E < 10$ GeV, it is known that solar wind can have significant effects on the charged particles, the so-called solar modulation which depends strongly on the solar activity. Since the uncertainty for the background flux in this range is large, we shall not discuss the spectra for $E < 10$ GeV any further in this paper. For $E > 10$ GeV the mass of X_μ and lifetime τ_{DM} are chosen to give relatively better fit with the data.

From green dotted lines of Fig. 9, we can see that $X^\mu \rightarrow e^+ e^-$ can not be consistent with positron fraction and the total flux simultaneously. The reason is that the spectrum of e^\pm from X_μ 's decay is very hard and too sharp around $E = M_X/2$, it is inconsistent with the Fermi total flux data. In case of $X_\mu \rightarrow \mu^+ \mu^-$, the situation is much better as shown in the blue dot-dashed lines for $M_X = 2$ TeV and $\tau_{\text{DM}} \simeq 2 \times 10^{26}$ s. Since the produced μ^\pm undergo subsequently three-body decay, $\mu^\pm \rightarrow e^\pm + \nu_e + \nu_\mu$, the resulting e^\pm spectrum from the muon decays is much softer.

In the $\tau^+ \tau^-$ case, the e^\pm spectrum is even softer than the $\mu^+ \mu^-$, since only one third of τ^\pm decay to μ^\pm and e^\pm . Other τ 's decay hadronically into lighter mesons which then decay further to pions, followed by $\pi^\pm \rightarrow \mu^\pm + \nu_\mu$ and $\pi^0 \rightarrow 2\gamma$. However, the spectrum's softness could be compensated with an even heavier X_μ . As we show in the brown double-dot-dashed lines of Figure. 9, $M_X = 7$ TeV and $\tau_{\text{DM}} \simeq 0.7 \times 10^{26}$ s can give a good fit with the data. We

shall note $m_X = 7$ TeV lies in the boundary of previous constraints as the perturbativity limits $g_X \lesssim 1.5$ which further set the upper bound $M_X \lesssim 7$ TeV to give correct relic density.

γ -ray Constraints: It is well known that the cosmic γ -ray is an important constraint on both pair-annihilating and decaying dark matters. If combined with gamma-ray constraint for decaying dark matter based on Fermi-LAT's released data [16, 18, 60–63], the only viable channel then is $X_\mu \rightarrow \mu^+ \mu^-$. The reasons are for $e^+ e^-$ channel all the lost energies goes to photons. For the $X_\mu \rightarrow \tau^+ \tau^-$ case, the decay products has a lot of π^0 which then all decay to 2γ , while for $X_\mu \rightarrow \mu^+ \mu^-$ a large part of muon energy is carried by the neutrinos in the decay product, leaving less energy for electron to radiate γ . Interpretation and constraints after AMS02 have been discussed in [19–36], which would not change the γ -ray constraints.

D. Parameter regions for thermal VDM with mass ~ 2 TeV

In this subsection, we summarize the parameter space of the renormalizable Lagrangian for thermal VDM with mass ~ 2 TeV which can account for the positron excess observed by PAMELA and AMS02 through its decays into $\mu^+ \mu^-$. As we have shown in sec. III, for $\mathcal{O}(\text{TeV})$ VDM X_μ the thermal relic density can pin down the gauge coupling $g_X \simeq 0.76$ in the dark sector (see Fig. 2 and Eq. 3.3). Then only M_{H_2} and the exact mixing angle α are left unfixed but correlated and constrained by Higgs data, DM direct searches, BBN and thermalization, displayed in Fig. 5. Taking $M_{H_2} \simeq 300\text{GeV}$ as an example, we have $\sin \alpha \lesssim 0.3$ and $\lambda_H \gtrsim 0.129$.

With all current constraints taken into account and when $M_{H_2} \geq 150\text{GeV}$, sizable deviation shown in Fig. 6 exists for the Higgs self-coupling, whose precise determination in the future colliders then could fix M_{H_2} and α , therefore predict the X_μ -nucleon cross section for DM direct searches and make our model testable. If we further require that our electroweak vacuum is stable up to the scale $\Lambda \sim 10^{15} - 10^{16}$ GeV, then all parameter space can be probed by XENON1T.

VI. SUMMARY

We have investigated the phenomenology of a vector dark matter X_μ in the framework of Higgs portal model, enlarging the SM gauge group G_{SM} by a dark $U(1)_X$. We first discuss the primary cosmic rays, including γ -ray and neutrino, from X_μ - X_μ annihilation and compare the spectra in several cases. In order to explain the recent interesting positron excess, we focus on the TeV scale M_X and show it can evade all the constraints from the Higgs data, relic density, perturbativity and dark matter direct search. Signals from heavy X_μ pair annihilation into leptons are well below the background and data. Since having the boost factor from the Sommerfeld enhancement is strongly constrained and basically ruled out by CMB, we then turn to the signatures from X_μ 's decay for explanation of the positron excess observed by PAMELA and AMS02.

We have also presented all the independent dimension-six operators that involve both standard model and dark sector particles, and that are invariant under the $G_{SM} \times U(1)_X$ gauge symmetry. After the breaking of $G_{SM} \times U(1)_X$, the VDM X_μ can decay to SM particles. A TeV X_μ can also explain the recent positron fraction excess observed in PAMELA, FERMI and AMS02. We give an example model to implement a leptophilic interaction and show the relevant indirect signature. It is shown that $X_\mu \rightarrow e^+ e^-$ gives a spectrum too hard

to explain the observation while $X_\mu \rightarrow \mu^+\mu^-$, $\tau^+\tau^-$ can be consistent with both positron fraction and total e^\pm flux. However, if taking the constraints from the gamma ray, then only $X_\mu \rightarrow \mu^+\mu^-$ is viable.

Our study presented in this paper is different from model independent analysis of cosmic rays in the literature, in that we demonstrated explicitly that thermalization of the VDM is possible for \sim TeV scale VDM, and then considered the VDM decays into a lepton pair. The indirect searches for cosmic rays can determine dark matter's mass, which then fixes the $U(1)_X$ gauge coupling for giving the thermal relic density. The only left two correlated parameters are the mass of second scalar and its mixing angle with Higgs. These two can be further probed by future collider searches, for instance, precision measurement of Higgs self coupling or production of the second scalar, and DM direct searches at XENON1T for example. The contents we have discussed systematically are complementary to each other and testable in terrestrial experiments, and similar analyses could be done for other types of decaying DM's assuming they were thermalized through some interactions.

Acknowledgments

This work is supported in part by National Research Foundation of Korea (NRF) Research Grant 2012R1A2A1A01006053 (SB,PK,WP,YT), and by the NRF grant funded by the Korea government (MSIP) (No. 2009-0083526) through Korea Neutrino Research Center at Seoul National University (PK).

-
- [1] P. A. R. Ade *et al.* [Planck Collaboration], arXiv:1303.5076 [astro-ph.CO].
 - [2] R. Kallosh, A. D. Linde, D. A. Linde and L. Susskind, Phys. Rev. D **52**, 912 (1995) [hep-th/9502069].
 - [3] T. Banks and N. Seiberg, Phys. Rev. D **83**, 084019 (2011) [arXiv:1011.5120 [hep-th]].
 - [4] S. Baek, P. Ko and W. -I. Park, JHEP **1307**, 013 (2013) [arXiv:1303.4280 [hep-ph]].
 - [5] L. Ackerman, M. R. Buckley, S. M. Carroll and M. Kamionkowski, Phys. Rev. D **79**, 023519 (2009) [arXiv:0810.5126 [hep-ph]]. J. L. Feng, M. Kaplinghat, H. Tu and H. -B. Yu, JCAP **0907**, 004 (2009) [arXiv:0905.3039 [hep-ph]]. D. E. Morrissey, D. Poland and K. M. Zurek, JHEP **0907**, 050 (2009) [arXiv:0904.2567 [hep-ph]]. O. Lebedev, H. M. Lee and Y. Mambrini, Phys. Lett. B **707**, 570 (2012) [arXiv:1111.4482 [hep-ph]].
 - [6] A. Djouadi, O. Lebedev, Y. Mambrini and J. Quevillon, Phys. Lett. B **709**, 65 (2012) [arXiv:1112.3299 [hep-ph]].
 - [7] T. Hambye, JHEP **0901**, 028 (2009) [arXiv:0811.0172 [hep-ph]].
 - [8] F. Chen, J. M. Cline and A. R. Frey, Phys. Rev. D **80**, 083516 (2009) [arXiv:0907.4746 [hep-ph]].
 - [9] H. Zhang, C. S. Li, Q. -H. Cao and Z. Li, Phys. Rev. D **82**, 075003 (2010) [arXiv:0910.2831 [hep-ph]].
 - [10] J. L. Diaz-Cruz and E. Ma, Phys. Lett. B **695**, 264 (2011) [arXiv:1007.2631 [hep-ph]].
 - [11] S. Baek, P. Ko and W. -I. Park, arXiv:1311.1035 [hep-ph].
 - [12] S. Baek, P. Ko, W. -I. Park and E. Senaha, JHEP **1305**, 036 (2013) [arXiv:1212.2131 [hep-ph]].
 - [13] O. Adriani *et al.* [PAMELA Collaboration], Nature **458**, 607 (2009) [arXiv:0810.4995 [astro-ph]].

- [14] A. A. Abdo *et al.* [Fermi LAT Collaboration], Phys. Rev. Lett. **102**, 181101 (2009) [arXiv:0905.0025 [astro-ph.HE]].
- [15] M. Aguilar *et al.* [AMS Collaboration], Phys. Rev. Lett. **110**, 141102 (2013).
- [16] M. Cirelli, M. Kadastik, M. Raidal and A. Strumia, Nucl. Phys. B **813**, 1 (2009) [Addendum-ibid. B **873**, 530 (2013)] [arXiv:0809.2409 [hep-ph]].
- [17] X. -J. Bi, X. -G. He and Q. Yuan, Phys. Lett. B **678**, 168 (2009) [arXiv:0903.0122 [hep-ph]].
- [18] M. Cirelli, P. Panci and P. D. Serpico, Nucl. Phys. B **840**, 284 (2010) [arXiv:0912.0663 [astro-ph.CO]].
- [19] L. Feng, R. -Z. Yang, H. -N. He, T. -K. Dong, Y. -Z. Fan and J. Chang, arXiv:1303.0530 [astro-ph.HE].
- [20] T. Bringmann, F. Calore, M. Di Mauro and F. Donato, arXiv:1303.3284 [astro-ph.CO].
- [21] L. Pearce and A. Kusenko, Phys. Rev. D **87**, 123531 (2013) [arXiv:1303.7294 [hep-ph]].
- [22] A. De Simone, A. Riotto and W. Xue, JCAP **1305**, 003 (2013) [JCAP **1305**, 003 (2013)] [arXiv:1304.1336 [hep-ph]].
- [23] Q. Yuan, X. -J. Bi, G. -M. Chen, Y. -Q. Guo, S. -J. Lin and X. Zhang, arXiv:1304.1482 [astro-ph.HE].
- [24] M. Ibe, S. Iwamoto, S. Matsumoto, T. Moroi and N. Yokozaki, JHEP **1308**, 029 (2013) [arXiv:1304.1483 [hep-ph]].
- [25] I. Cholis and D. Hooper, Phys. Rev. D **88**, 023013 (2013) [arXiv:1304.1840 [astro-ph.HE]].
- [26] H. -B. Jin, Y. -L. Wu and Y. -F. Zhou, arXiv:1304.1997 [hep-ph].
- [27] Y. Kajiyama, H. Okada and T. Toma, arXiv:1304.2680 [hep-ph].
- [28] Q. Yuan and X. -J. Bi, arXiv:1304.2687 [astro-ph.HE].
- [29] I. Masina and F. Sannino, Phys. Rev. D **87**, 123003 (2013) [arXiv:1304.2800 [hep-ph]].
- [30] P. -F. Yin, Z. -H. Yu, Q. Yuan and X. -J. Bi, Phys. Rev. D **88**, 023001 (2013) [arXiv:1304.4128 [astro-ph.HE]].
- [31] L. Feng and Z. Kang, arXiv:1304.7492 [hep-ph].
- [32] Z. -P. Liu, Y. -L. Wu and Y. -F. Zhou, arXiv:1305.5438 [hep-ph].
- [33] K. R. Dienes, J. Kumar and B. Thomas, arXiv:1306.2959 [hep-ph].
- [34] L. Bergstrom, T. Bringmann, I. Cholis, D. Hooper and C. Weniger, [arXiv:1306.3983 [astro-ph.HE]].
- [35] A. Ibarra, A. S. Lamperstorfer and J. Silk, arXiv:1309.2570 [hep-ph].
- [36] C. -Q. Geng, D. Huang and L. -H. Tsai, arXiv:1312.0366 [hep-ph].
- [37] C. -R. Chen, M. M. Nojiri, F. Takahashi and T. T. Yanagida, Prog. Theor. Phys. **122**, 553 (2009) [arXiv:0811.3357 [astro-ph]].
- [38] E. J. Chun, J. -C. Park and S. Scopel, JHEP **1102**, 100 (2011) [arXiv:1011.3300 [hep-ph]].
- [39] S. Y. Choi, C. Englert and P. M. Zerwas, arXiv:1308.5784 [hep-ph].
- [40] H. Davoudiasl and I. M. Lewis, arXiv:1309.6640 [hep-ph].
- [41] S. Choi, S. Jung and P. Ko, arXiv:1307.3948 [hep-ph].
- [42] E. Aprile *et al.* [XENON100 Collaboration], Phys. Rev. Lett. **109**, 181301 (2012) [arXiv:1207.5988 [astro-ph.CO]].
- [43] D. S. Akerib *et al.* [LUX Collaboration], arXiv:1310.8214 [astro-ph.CO].
- [44] G. Belanger, F. Boudjema, A. Pukhov and A. Semenov, arXiv:1305.0237 [hep-ph].
- [45] G. Bertone, J. Silk, B. Moore, J. Diemand, J. Bullock, M. Kaplinghat, L. Strigari and Y. Mellier *et al.*, Cambridge, UK: Univ. Pr. (2010) 738 p
- [46] J. F. Navarro, C. S. Frenk and S. D. M. White, Astrophys. J. **490**, 493 (1997) [astro-ph/9611107].

- [47] A. Ibarra, D. Tran and C. Weniger, JCAP **1001**, 009 (2010) [arXiv:0906.1571 [hep-ph]].
- [48] J. Hisano, S. Matsumoto, M. Nagai, O. Saito and M. Senami, Phys. Lett. B **646**, 34 (2007) [hep-ph/0610249].
- [49] N. Arkani-Hamed, D. P. Finkbeiner, T. R. Slatyer and N. Weiner, Phys. Rev. D **79**, 015014 (2009) [arXiv:0810.0713 [hep-ph]].
- [50] J. Hisano, S. Matsumoto, M. M. Nojiri and O. Saito, Phys. Rev. D **71**, 063528 (2005) [hep-ph/0412403].
- [51] M. Ibe, H. Murayama and T. T. Yanagida, Phys. Rev. D **79**, 095009 (2009) [arXiv:0812.0072 [hep-ph]].
- [52] W. -L. Guo and Y. -L. Wu, Phys. Rev. D **79**, 055012 (2009) [arXiv:0901.1450 [hep-ph]].
- [53] S. Galli, F. Iocco, G. Bertone and A. Melchiorri, Phys. Rev. D **80**, 023505 (2009) [arXiv:0905.0003 [astro-ph.CO]].
- [54] T. R. Slatyer, N. Padmanabhan and D. P. Finkbeiner, Phys. Rev. D **80**, 043526 (2009) [arXiv:0906.1197 [astro-ph.CO]].
- [55] W. Buchmuller and D. Wyler, Nucl. Phys. B **268**, 621 (1986).
- [56] B. Grzadkowski, M. Iskrzynski, M. Misiak and J. Rosiek, JHEP **1010**, 085 (2010) [arXiv:1008.4884 [hep-ph]].
- [57] M. Gustafsson, T. Hambye and T. Scarna, Phys. Lett. B **724**, 288 (2013) [arXiv:1303.4423 [hep-ph]].
- [58] C. Arina, T. Hambye, A. Ibarra and C. Weniger, JCAP **1003**, 024 (2010) [arXiv:0912.4496 [hep-ph]].
- [59] S. Baek and P. Ko, JCAP **0910**, 011 (2009) [arXiv:0811.1646 [hep-ph]].
- [60] M. Ackermann *et al.* [LAT Collaboration], Phys. Rev. D **86**, 022002 (2012) [arXiv:1205.2739 [astro-ph.HE]].
- [61] M. Ackermann *et al.* [LAT Collaboration], Astrophys. J. **761**, 91 (2012) [arXiv:1205.6474 [astro-ph.CO]].
- [62] M. Cirelli, E. Moulin, P. Panci, P. D. Serpico and A. Viana, Phys. Rev. D **86**, 083506 (2012) [arXiv:1205.5283 [astro-ph.CO]].
- [63] G. A. Gomez-Vargas, M. A. Sanchez-Conde, J. -H. Huh, M. Peiro, F. Prada, A. Morselli, A. Klypin and D. G. Cerdeno *et al.*, arXiv:1308.3515 [astro-ph.HE].